The 8th European Congress on Computational Methods in Applied Sciences and Engineering
ECCOMAS Congress 2022
5-9 June 2022, Oslo, Norway

A SEMI-IMPLICIT METHOD FOR THROMBUS FORMATION IN HAEMODYNAMIC FLUID–STRUCTURE INTERACTION

Richard Schussnig[1,2], Simon Dreymann[2,3], Alireza Jafarinia[2,3], Thomas Hochrainer[2,3] and Thomas-Peter Fries[1,2]

[1] Institute of Structural Analysis, Graz University of Technology,
Lessingstraße 25/II, 8010 Graz, Austria, ifb.tugraz.at

[2] Graz Center of Computational Engineering, Graz University of Technology,
Krenngasse 37/I, 8010 Graz, Austria, gcce.tugraz.at

[3] Institute of Strength of Materials, Graz University of Technology,
Kopernikusgasse 24/I, 8010 Graz, Austria, ifl.tugraz.at

Key words: Thrombus Formation, Blood Flow, Incompressible Fluid–Structure Interaction, Navier–Stokes Equations, Time-Splitting Scheme, Pressure Poisson Equation

Abstract. Aortic flows with thrombus formation represent a challenging application of fluid-structure interaction (FSI) in biomechanics where blood flow, thrombus, and vessel wall are strongly coupled. Considering patient-specific FSI and thrombus formation on identical time scales remains unfeasible. To resolve this issue, we propose incorporating the dynamics-based thrombus formation model of Menichini et al. [1] into our recently presented semi-implicit, split-step partitioned FSI scheme for non-Newtonian fluids [2, 3]. Herein, we formulate the basic split-step scheme and present the first promising results, merely coupling the fluid pressure and structure displacement iteratively at each time step.

1 INTRODUCTION

Blood clotting and thrombus formation play a key role in many cardiovascular diseases, drastically impacting surgical planning and options, risk factors, and possible long-term treatment. Thrombosis significantly impacts the flow field and is thus a major design criterion for, e.g., blood pumps or implants such as stents or artificial valves. In such scenarios, vast changes in the affected flow regions are triggered, but can only be captured considering the tight coupling of fluid flow, thrombus build-up and tissue deformation within a fluid–structure interaction (FSI) framework. However, for modern computational methods to aid clinical decision-making or highlight risks associated with individual interventions, efficient algorithms are needed. Computational modeling of thrombus formation has remained challenging in this regard despite the advances in computational biomechanics during the past decade, since it combines demanding fluid flow or FSI problems with complex biochemical systems.

To render such problems feasible, we combine (i) a split-step method for incompressible non-Newtonian FSI [2], which was extended by interface quasi-Newton acceleration, suitable

Robin interface conditions, and other models and numerical aspects in [3] with (ii) the thrombus formation model of Menichini et al. [1]. A semi-implicit FSI scheme allows coupling only the bulk elastic structure's displacement and the fluid pressure iteratively, while the equations governing constituent transport and all other fields are solved only once per time step. Herein, the first results in a clinically relevant setting are presented to highlight the efficiency and applicability of the framework. Of particular interest are the coupling to a dynamics-based thrombus model, decoupling the FSI time scale and accelerating the thrombus growth scale based on averaged haemodynamic quantities. The considered fluid, solid and thrombus formation models can be seen as placeholders, which can be replaced by similar approaches.

2 PROBLEM STATEMENT

The instationary domain Ω^t at time $t \in (0, T]$ is composed of subdomains Ω_f^t and Ω_s^t denoting the volume occupied by the fluid and structure phases, where $\Omega^t = \Omega_f^t \cup \Omega_s^t$. Adopting an Arbitrary Lagrangian–Eulerian (ALE) method, the fluid domain at current time t is considered, based on the corresponding entities in the reference configuration, $\hat{\Omega} = \hat{\Omega}_f \cup \hat{\Omega}_s$. The fluid–structure interface is denoted by $\Sigma^t := \partial\Omega_f^t \cap \partial\Omega_s^t$ in the spatial configuration, while in the reference frame, we have $\hat{\Sigma} := \partial\hat{\Omega}_f \cap \partial\hat{\Omega}_s$. In both the fluid and structure subdomains, mappings from the reference to the spatial configuration are constructed,

$$\mathcal{A}^t : \hat{\Omega}_f \to \Omega_f^t, \qquad \mathcal{A}^t := \hat{\boldsymbol{x}} + \boldsymbol{d}_f(\hat{\boldsymbol{x}}, t), \qquad \boldsymbol{F}_f := \boldsymbol{I} + \hat{\nabla}\boldsymbol{d}_f, \qquad J_f := \det \boldsymbol{F}_f, \tag{1}$$

$$\mathcal{L}^t : \hat{\Omega}_s \to \Omega_s^t, \qquad \mathcal{L}^t := \hat{\boldsymbol{x}} + \boldsymbol{d}_s(\hat{\boldsymbol{x}}, t), \qquad \boldsymbol{F}_s := \boldsymbol{I} + \hat{\nabla}\boldsymbol{d}_s, \qquad J_s := \det \boldsymbol{F}_s, \tag{2}$$

in terms of the fluid and structure displacements $\boldsymbol{d}_f$ and $\boldsymbol{d}_s$. Further, we introduce the deformation gradients $\boldsymbol{F}_f$ and $\boldsymbol{F}_s$ and their determinants J_f and J_s, emphasising by $\hat{}$ the connection to $\hat{\Omega}$ whenever necessary. On the interface, there holds

$$\boldsymbol{d}_s = \boldsymbol{d}_f, \qquad \mathrm{d}_t\boldsymbol{d}_s = \boldsymbol{u}_f, \qquad \boldsymbol{P}\,\hat{\boldsymbol{n}}_s = J_f\boldsymbol{\sigma}_f\boldsymbol{F}_f^{-\top}\hat{\boldsymbol{n}}_s \quad \text{on } \hat{\Sigma}, \tag{3}$$

i.e., continuity of displacements, velocities, and tractions hold. Here, $\mathrm{d}_t\boldsymbol{d}_s$ denotes the solid's material velocity, $\boldsymbol{P}$ the first Piola–Kirchhoff stress tensor, $\boldsymbol{\sigma}_f$ the fluid's Cauchy stress tensor and $\hat{\boldsymbol{n}}_s$ the unit outward normal of $\hat{\Omega}_s$. Following the ALE approach, smoothly extending $\boldsymbol{d}_f$ from given $\boldsymbol{d}_s$ on $\hat{\Sigma}$ into $\hat{\Omega}_f$ is crucial. So, we consider an auxiliary problem,

$$-\hat{\nabla} \cdot \left[\lambda_m(\hat{\nabla} \cdot \boldsymbol{d}_f)\boldsymbol{I} + 2\mu_m\hat{\nabla}^{\mathrm{S}}\boldsymbol{d}_f\right] = \boldsymbol{0} \qquad \text{in } \hat{\Omega}_f, \tag{4}$$

$$\boldsymbol{d}_f = \boldsymbol{d}_s \qquad \text{on } \hat{\Sigma}, \tag{5}$$

$$\boldsymbol{d}_f = \boldsymbol{0} \qquad \text{on } \partial\hat{\Omega}_f \setminus \hat{\Sigma}, \tag{6}$$

with the symmetric gradient $2\hat{\nabla}^{\mathrm{S}} := \hat{\nabla}^\top + \hat{\nabla}$, describing the deformation of a linear elastic continuum. In (4), the Lamé parameters λ_m and μ_m are locally modified depending on the element size h_e and Jacobian J_f (see, e.g., [5]). Then, $\mathcal{A}^t$, $\boldsymbol{F}_f$ and J_f are given by (1), while in

the solid domain $\hat{\Omega}_s$, the material displacement is governed by

$$\rho_s \mathrm{d}_t^2 \boldsymbol{d}_s - \hat{\nabla} \cdot \boldsymbol{P} = \boldsymbol{b}_s \qquad \text{in } \hat{\Omega}_s, \tag{7}$$

$$\eta_s^R \mathrm{d}_t \boldsymbol{d}_f + \boldsymbol{P}\,\hat{\boldsymbol{n}}_s = \eta_s^R \boldsymbol{u}_f + J_f \boldsymbol{\sigma}_f \boldsymbol{F}_f^{-\top} \hat{\boldsymbol{n}}_s \qquad \text{on } \hat{\Sigma}, \tag{8}$$

$$\boldsymbol{P}\,\hat{\boldsymbol{n}}_s = -k_e \boldsymbol{d}_s - c_e \mathrm{d}_t \boldsymbol{d}_s \qquad \text{on } \hat{\Gamma}_{R,s}, \tag{9}$$

$$\boldsymbol{d}_s = \boldsymbol{0} \qquad \text{on } \hat{\Gamma}_{D,s}, \tag{10}$$

using a total Lagrangian approach and given suitable initial conditions for $\mathrm{d}_t \boldsymbol{d}_s$ and $\boldsymbol{d}_s$. Here, ρ_s denotes the structure's density, $\mathrm{d}_t^2 \boldsymbol{d}_s$ the material acceleration, $\boldsymbol{b}_s$ the body force, (8) is a Robin interface condition with parameter η_s^R, incorporating the fluid's velocity $\boldsymbol{u}_f$ and (9) accounts for viscoelastic support with coefficients k_e and c_e. Robin interface conditions as (8) have been shown to accelerate and stabilise the fluid–structure coupling also in cases with high added-mass effect [6]. The structure's constitutive law is for simplicity chosen as

$$\boldsymbol{P} := \lambda_s (\hat{\nabla} \cdot \boldsymbol{d}_s) \boldsymbol{I} + 2\mu_s \hat{\nabla}^{\mathrm{S}} \boldsymbol{d}_s, \tag{11}$$

that is, linear elasticity. This simplification is in general too strict, as one might want to consider for nonlinear material behaviour, incompressibility and/or anisotropic fiber reinforcement [3]. However, we can justify its use within this contribution, given that the focus lies on the FSI coupling algorithm, including thrombus formation, and in a partitioned setup, (11) is easily replaced, as (3) and (8) account for large strains.

For a generalised Newtonian fluid, the Cauchy stress $\boldsymbol{\sigma}_f$ is given by

$$\boldsymbol{\sigma}_f := -p_f \boldsymbol{I} + 2\mu_f \nabla^{\mathrm{S}} \boldsymbol{u}_f, \tag{12}$$

where p_f denotes the fluid's pressure, and the dynamic viscosity μ_f depends on the shear rate $\dot{\gamma}(\nabla^{\mathrm{S}} \boldsymbol{u}_f)$. The shear-thinning behaviour of blood is captured via Carreau's law,

$$\eta(\dot{\gamma}) = \eta_\infty + (\eta_0 - \eta_\infty) \left[1 + (\lambda_f \dot{\gamma})^2\right]^{\frac{\xi-1}{2}}, \quad \text{with } \dot{\gamma} := \sqrt{1/2 \nabla^{\mathrm{S}} \boldsymbol{u}_f : \nabla^{\mathrm{S}} \boldsymbol{u}_f}, \tag{13}$$

with suitable upper and lower viscosity limits η_0 and η_∞ and fitting parameters λ_f and ξ.

The classical ALE form of the Navier–Stokes equations for incompressible flows of generalised Newtonian fluids on the moving domain Ω_f^t can then be reformulated as

$$\boldsymbol{b}_f = \rho_f \left[\partial_t \boldsymbol{u}_f|_{\tilde{\boldsymbol{x}}} + \nabla \boldsymbol{u}_f (\boldsymbol{u}_f - \boldsymbol{u}_m)\right] - \nabla \cdot \boldsymbol{\sigma}_f \qquad \text{in } \Omega_f^t, \tag{14}$$

$$-\Delta p_f = \nabla \cdot \left[\rho_f \nabla \boldsymbol{u}_f (\boldsymbol{u}_f - \boldsymbol{u}_m) - 2\nabla^{\mathrm{S}} \boldsymbol{u}_f \nabla \mu_f - \boldsymbol{b}_f\right] + \left[\nabla \times (\nabla \times \boldsymbol{u}_f)\right] \cdot \nabla \mu_f \qquad \text{in } \Omega_f^t, \tag{15}$$

$$\boldsymbol{u}_f = \mathrm{d}_t \boldsymbol{d}_s \qquad \text{on } \Sigma^t, \tag{16}$$

$$\boldsymbol{u}_f = \boldsymbol{g}_f \qquad \text{on } \Gamma_{D,f}^t, \tag{17}$$

$$\boldsymbol{\sigma}_f \boldsymbol{n}_f = \boldsymbol{t}_f \qquad \text{on } \Gamma_{N,f}^t, \tag{18}$$

$$p_f = -\mu_f \nabla \cdot \boldsymbol{u}_f + \boldsymbol{n}_f \cdot \left(2\mu_f \nabla^{\mathrm{S}} \boldsymbol{u}_f \boldsymbol{n}_f - \boldsymbol{t}_f\right) \qquad \text{on } \Gamma_{N,f}^t, \tag{19}$$

$$\boldsymbol{n}_f \cdot \nabla p_f = \boldsymbol{n}_f \cdot \left[\boldsymbol{b}_f + 2\nabla^{\mathrm{S}} \boldsymbol{u}_f \nabla \mu_f - \mu_f \nabla \times (\nabla \times \boldsymbol{u}_f) - \rho_f \nabla \boldsymbol{u}_f (\boldsymbol{u}_f - \boldsymbol{u}_m) - \rho_f \partial_t \boldsymbol{g}_f|_{\tilde{\boldsymbol{x}}}\right] \qquad \text{on } \Gamma_{D,f}^t, \tag{20}$$

$$\boldsymbol{n}_f \cdot \nabla p_f = \boldsymbol{n}_f \cdot \left[\boldsymbol{b}_f + 2\nabla^{\mathrm{S}} \boldsymbol{u}_f \nabla \mu_f - \mu_f \nabla \times (\nabla \times \boldsymbol{u}_f) - \rho_f \nabla \boldsymbol{u}_f (\boldsymbol{u}_f - \boldsymbol{u}_m) - \rho_f \mathrm{d}_t^2 \boldsymbol{d}_s\right] \qquad \text{on } \Sigma^t, \tag{21}$$

where the interested reader is referred to [2, 4] for further details. Herein, $\boldsymbol{b}_f$ denotes the body force, ρ_f the fluid's density, $\partial_t \boldsymbol{u}_f|_{\tilde{\boldsymbol{x}}}$ the ALE time derivative, $\boldsymbol{u}_m$ the mesh velocity $\boldsymbol{u}_m := \partial_t \boldsymbol{d}_f|_{\tilde{\boldsymbol{x}}}$. Note that all spatial derivatives are taken with respect to $\boldsymbol{x}$ and we consider the current domain Ω_f^t, while $\partial_t|_{\tilde{\boldsymbol{x}}}$ uses data corresponding to grid points of the moving mesh.

The system (14)–(21) consists of the standard momentum balance equation (14), a pressure Poisson equation (PPE) replacing the divergence-free constraint by (15), and is equipped with fully consistent boundary conditions for both the velocity and pressure (16)–(21). Starting from this system, efficient semi-implicit schemes can be derived, considering for pure flow problems, the PPE and momentum balance equations only need to be solved once per time step, while in the FSI setting, this choice allows employing efficient and added-mass stable coupling schemes, merely coupling the fluid pressure and structure displacement iteratively, see Sec. 3.

We assume suitable initial conditions given for all unknowns including p_f, which is trivial starting from the quiescent state, $\boldsymbol{u}_f = \boldsymbol{0}$, and using zero body force, $\boldsymbol{b}_f = \boldsymbol{0}$, or alternatively construct μ_f and p_f based on a given velocity field $\boldsymbol{u}_f$ by projecting the rheological law (12) and solving the PPE (15) before starting the split-step scheme.

Even though the system (14)–(21) inherently enforces $\nabla \cdot \boldsymbol{u}_f$, i.e., incompressibility without any modification, mass conservation is further improved by so-called divergence damping [4]. Divergence damping is rooted in a Helmholtz-Leray decomposition $\boldsymbol{u}_f := \check{\boldsymbol{u}}_f + \nabla\psi$, constructing a weakly divergence-free velocity field via

$$-\Delta\psi = -\nabla \cdot \boldsymbol{u}_f \qquad \text{in } \Omega_f^t, \tag{22}$$

$$\boldsymbol{n}_f \cdot \nabla\psi = 0 \qquad \text{on } \Gamma_{D,f}^t \cup \Sigma^t, \tag{23}$$

$$\psi = 0 \qquad \text{on } \Gamma_{N,f}^t, \tag{24}$$

but considering the auxiliary variable ψ on the past time step's velocities only. This way, velocity boundary conditions are preserved at t^{n+1}, an additional velocity projection step is circumvented and the auxiliary Poisson problem (22)–(24) is only solved once per time step given $\boldsymbol{u}_f$.

Lastly, let us briefly introduce the thrombus formation model by Menichini et al. [1]. One of the main ingredients of the thrombus formation model is the particle residence time τ, which is governed by a convection–diffusion–reaction equation,

$$\partial_t \tau|_{\tilde{\boldsymbol{x}}} + (\boldsymbol{u}_f - \boldsymbol{u}_m) \cdot \nabla\tau - D_\tau \Delta\tau = 1 \qquad \text{in } \Omega_f^t, \tag{25}$$

$$\tau = 0 \qquad \text{on } \Gamma_{D,f}^t, \tag{26}$$

$$\boldsymbol{n}_f \cdot \nabla\tau = 0 \qquad \text{on } \partial\Omega_f^t \setminus \Gamma_{D,f}^t, \tag{27}$$

and zero initial condition in the whole domain, i.e., $\tau = 0$ in Ω_f^t. The self-diffusivity of blood is $D_\tau = 1.14 \times 10^{-14}\ \mathrm{m^2/s}$, such that the convective and reactive terms dominate, possibly triggering spurious oscillations when employing a finite element method as discussed in Sec. 3.

Within the thrombus model, time-averaged haemodynamics are considered via mean values over the previous cardiac cycle i of length T_p from $t_p^{i-1} := (i-1)T_p$ to $t_p^i := i\,T_p$ of the residence time τ, shear rate $\dot{\gamma}$ and shear stress vector $\boldsymbol{s} := \boldsymbol{S}\boldsymbol{n} - [(\boldsymbol{S}\boldsymbol{n}) \cdot \boldsymbol{n}]\,\boldsymbol{n}$ as

$$\overline{\tau} := \frac{1}{T_p \max\{\tau|_{t=t_p^i}\}} \int_{t_p^{i-1}}^{t_p^i} \tau|_{\tilde{\boldsymbol{x}}}\,\mathrm{d}t, \qquad \overline{\gamma} := \frac{1}{T_p} \int_{t_p^{i-1}}^{t_p^i} \dot{\gamma}|_{\tilde{\boldsymbol{x}}}\,\mathrm{d}t, \qquad \overline{\boldsymbol{s}} := \frac{1}{T_p} \int_{t_p^{i-1}}^{t_p^i} \boldsymbol{s}|_{\tilde{\boldsymbol{x}}}\,\mathrm{d}t, \tag{28}$$

which are variable fields in Ω_f^t and on $\partial\Omega_f^t$, respectively, to be used in the following cardiac cycle. These quantities are then used to identify regions of high residence time and low shear, favouring coagulation and thrombus build-up. Based on the residence time, the concentration of activated and resting platelets, c_a and c_r, is determined solving

$$\partial_t c_a|_{\tilde{\boldsymbol{x}}} + (\boldsymbol{u}_f - \boldsymbol{u}_m)\cdot\nabla c_a - D_p\Delta c_a = (\alpha_1 c_a + \alpha_2\overline{\tau})\, c_r \qquad \text{in } \Omega_f^t, \tag{29}$$

$$\partial_t c_r|_{\tilde{\boldsymbol{x}}} + (\boldsymbol{u}_f - \boldsymbol{u}_m)\cdot\nabla c_r - D_p\Delta c_r = (\alpha_3 c_a + \alpha_4\overline{\tau})\, c_r \qquad \text{in } \Omega_f^t, \tag{30}$$

$$c_a = c_r = 0 \qquad \text{on } \Gamma_{D,f}^t, \tag{31}$$

$$\boldsymbol{n}\cdot\nabla c_a = \boldsymbol{n}\cdot\nabla c_r = 0 \qquad \text{on } \partial\Omega_f^t \setminus \Gamma_{D,f}^t, \tag{32}$$

with a uniform initial condition $c_a = c_r = 1$ in Ω_f^t at $t = 0$. The enhanced Brownian diffusivity is $D_p = 1.6\,(1+\dot{\gamma}) \times 10^{-13}$ m^2/s and the coefficients are $(\alpha_1, \alpha_2, \alpha_3, \alpha_4) = (3, 10, 0.15, 0.5)$ $1/\mathrm{s}$. Further, introducing the scaled quantities

$$\tilde{c}_b := \frac{c_b^2}{c_b^2 + 4\times 10^8}, \quad \tilde{\gamma} := \frac{\overline{\gamma}^2}{\overline{\gamma}^2 + 250}, \quad \tilde{c}_c := \frac{c_c^2}{c_c^2 + 10^8}, \quad \tilde{\tau} := \frac{\overline{\tau}^2}{\overline{\tau}^2 + 0.81}, \tag{33}$$

write the system governing the coagulant c_c and bound platelets c_b concentrations as

$$\partial_t c_c|_{\tilde{\boldsymbol{x}}} - D_c\Delta c_c = k_c\tilde{c}_b\tilde{\gamma} \qquad \text{in } \Omega_f^t \tag{34}$$

$$\partial_t c_b|_{\tilde{\boldsymbol{x}}} = k_b\tilde{c}_c\tilde{\tau}\tilde{\gamma}\, c_a \qquad \text{in } \Omega_f^t, \tag{35}$$

$$c_c = 0 \qquad \text{on } \partial\Omega_f^t \setminus \Gamma_c^t. \tag{36}$$

On $\Gamma_c^t \subset \Sigma^t$, a conditional Neumann term for the coagulant concentration c_c is enforced,

$$\boldsymbol{n}\cdot\nabla c_c = q_c := \begin{cases} k_w & \text{if } ||\overline{\boldsymbol{s}}|| < 0.2 \text{ Pa} \wedge c_b < 2\times 10^5 \ \mathrm{nmol}/\mathrm{m}^3 \\ 0 & \text{otherwise} \end{cases} \qquad \text{on } \Gamma_c^t, \tag{37}$$

such that the coagulant concentration is increased on Γ_c^t under low wall shear stress conditions combined with a low concentration of bound platelets. The diffusion and coupling coefficients in (34)–(37) are given as $D_c = 1.6\,\tilde{\gamma} \times 10^{-8}$ m^2/s and $(k_b, k_c, k_w) = (1, 2, 0.02) \times 10^6$ $\mathrm{nmol}/\mathrm{m}^3$.

Having introduced all the thrombus constituents and the necessary auxiliary flow quantities, the modification to the Navier–Stokes equations and hence the equivalent system in (14)–(21) is small: it only consists of modifying the volumetric source term $\boldsymbol{b}_f \leftarrow \boldsymbol{b}_f - k\tilde{c}_b\boldsymbol{u}_f$, where $k = 10^7 \times \mathrm{kg}/\mathrm{m}^3\mathrm{s}$ inhibits fluid flow in regions of high bound platelet concentration. In fact, one might exchange the flow solver by one's favourite choice, merely adapting the source term and considering the additional convection–diffusion–reaction equations modeling thrombus growth. In the following, however, the modular nature of split-step scheme will be exploited by thoughtful use of extrapolation/linearisation, deriving an added-mass stable FSI scheme.

3 DISCRETISATION

We decompose the interval $(0, T]$ into N_t time steps of length $\Delta t^n = t^{n+1} - t^n$, $n = 0, \ldots, N_t$ and employ the Chung–Hulbert-α time integrator [7] for the structure, yielding

$$\rho_s\left(\alpha'_{\mathrm{m}}\ddot{\boldsymbol{d}}_s^{n+1} + \alpha_{\mathrm{m}}\ddot{\boldsymbol{d}}_s^{n}\right) - \alpha'_{\mathrm{f}}\hat{\nabla}\cdot\boldsymbol{P}\left(\boldsymbol{d}_s^{n+1}\right) - \alpha_{\mathrm{f}}\hat{\nabla}\cdot\boldsymbol{P}\left(\boldsymbol{d}_s^{n}\right) = \alpha'_{\mathrm{f}}\boldsymbol{b}_s^{n+1} + \alpha_{\mathrm{f}}\boldsymbol{b}_s^{n} \qquad \text{in } \hat{\Omega}_s, \tag{38}$$

where $\alpha'_{\mathrm{m}} = 1 - \alpha_{\mathrm{m}}$ and $\alpha'_{\mathrm{f}} = 1 - \alpha_{\mathrm{f}}$ and a generalised trapezoidal rule is applied to the stress–divergence terms. The structure's acceleration $\ddot{\boldsymbol{d}}_s$ and velocity $\dot{\boldsymbol{d}}_s$ are given by

$$\ddot{\boldsymbol{d}}_s^{n+1} = \frac{1}{\beta \Delta t^2} \left(\boldsymbol{d}_s^{n+1} - \boldsymbol{d}_s^n \right) - \frac{1}{\beta \Delta t} \dot{\boldsymbol{d}}_s^n + \left(1 - \frac{1}{2\beta} \right) \ddot{\boldsymbol{d}}_s^n , \tag{39}$$

$$\dot{\boldsymbol{d}}_s^{n+1} = \frac{\gamma}{\beta \Delta t} \left(\boldsymbol{d}_s^{n+1} - \boldsymbol{d}_s^n \right) - \left(1 - \frac{\gamma}{\beta} \right) \dot{\boldsymbol{d}}_s^n + \Delta t \left(1 - \frac{\gamma}{2\beta} \right) \ddot{\boldsymbol{d}}_s^n , \tag{40}$$

with $\gamma = \frac{1}{2} - \alpha_{\mathrm{m}} + \alpha_{\mathrm{f}}$, $\beta = \frac{1}{4} \left(1 - \alpha_{\mathrm{m}} + \alpha_{\mathrm{f}} \right)^2$, $\alpha_{\mathrm{f}} := \frac{2\rho_\infty - 1}{1 + \rho_\infty}$ and $\alpha_{\mathrm{m}} := \frac{\rho_\infty}{1 + \rho_\infty}$, depending on the spectral radius in the high frequency limit ρ_∞.

For the fluid and thrombus subproblems, we use backward differentiation formulae (BDF) of order m, which gives, e.g., for the residence time τ and fluid velocity $\boldsymbol{u}_f$

$$\partial_t \tau |_{\tilde{\boldsymbol{x}}} \approx \sum_{j=0}^{m} \alpha_j^m \tau^{n+1-j} , \quad \partial_t \boldsymbol{u}_f |_{\tilde{\boldsymbol{x}}} \approx \alpha_0^m \boldsymbol{u}_f^{n+1} + \sum_{j=0}^{m-1} \alpha_{j+1}^m \left(\boldsymbol{u}_f^{n-j} - \nabla \psi^{n-j} \right) , \tag{41}$$

which are to be understood in an ALE sense and where $\partial_t \boldsymbol{u}_f |_{\tilde{\boldsymbol{x}}}$ includes divergence damping terms on the past time step's solutions via the auxiliary variable ψ.

A key aspect of the proposed split-step scheme is the linearisation and decoupling of the fluid's velocity and pressure, which allows to recover them independently. For this reason, extrapolations of the same order m are introduced as

$$p_f^{n+1} \approx p_f^\star = \sum_{j=1}^{m} \beta_j^m p_f , \quad \boldsymbol{u}_f^{n+1} \approx \boldsymbol{u}_f^\star = \sum_{j=1}^{m} \beta_j^m \boldsymbol{u}_f , \tag{42}$$

and likewise for all other involved variables. The coefficients α_j^m and β_j^m for BDF time integration and extrapolation of order $m = 1$ and $m = 2$ are given in Tab. 1.

Table 1: Coefficients for BDF schemes, α_j^m, and extrapolation, β_j^m.

m	1	1	2	2	2
j	0	1	0	1	2
α_j^m	$\frac{1}{\Delta t^n}$	$-\frac{1}{\Delta t^n}$	$\frac{2\Delta t^n + \Delta t^{n-1}}{\Delta t^n (\Delta t^n + \Delta t^{n-1})}$	$-\frac{\Delta t^n + \Delta t^{n-1}}{\Delta t^n \Delta t^{n-1}}$	$\frac{\Delta t^n}{\Delta t^{n-1} (\Delta t^n + \Delta t^{n-1})}$
β_j^m	$\times$	1	$\times$	$1 + \frac{\Delta t^n}{\Delta t^{n-1}}$	$\frac{\Delta t^n}{\Delta t^{n-1}}$

Discretisation in space is carried out employing standard, C^0-continuous Lagrangian finite elements were suitable weak forms of all the involved balance equations are constructed following [2, 4], allowing for equal-order interpolation of velocity and pressure. The PPE-based split-step scheme circumvents the inf-sup condition such that first-order finite element spaces can be employed to discretise the weak forms.

The weak formulation of the pseudo elasticity problem (4)–(6) at the center of the ALE mesh update step, reads: Find $\boldsymbol{d}_f^{n+1} \in [H^1(\hat{\Omega}_f)]^d$, such that $\boldsymbol{d}_f^{n+1}|_{\hat{\Sigma}} = \boldsymbol{d}_s^\star$ and $\boldsymbol{d}_f^{n+1}|_{\partial\hat{\Omega}_f \setminus \hat{\Sigma}} = \boldsymbol{0}$ and

$$\left\langle \hat{\nabla} \boldsymbol{\varphi}, \lambda_m (\hat{\nabla} \cdot \boldsymbol{d}_f^{n+1}) \boldsymbol{I} + 2\mu_m \hat{\nabla}^{\mathrm{S}} \boldsymbol{d}_f^{n+1} \right\rangle_{\hat{\Omega}_f} = 0 \qquad \forall \boldsymbol{\varphi} \in [H^1(\hat{\Omega}_f)]^d, \text{ with } \boldsymbol{\varphi}|_{\partial\hat{\Omega}_f} = \boldsymbol{0}, \tag{43}$$

which can then be used to update $\boldsymbol{u}_m = \partial_t \boldsymbol{d}_f|_{\tilde{\boldsymbol{x}}}$ via (41). Similarly, a weak form corresponding to the structure's momentum balance equation is: Find $\boldsymbol{d}_s^{k+1} \in [H^1(\hat{\Omega}_s)]^d$ with $\boldsymbol{d}_s^{k+1}|_{\hat{\Gamma}_{D,s}} = \boldsymbol{g}_s^{n+1}$, such that for all $\boldsymbol{\varphi} \in [H^1(\hat{\Omega}_s)]^d$ with $\boldsymbol{\varphi}|_{\hat{\Gamma}_{D,s}} = \boldsymbol{0}$, there holds:

$$\begin{aligned}
&\rho_s \left\langle \boldsymbol{\varphi}, \alpha'_{\mathrm{m}} \ddot{\boldsymbol{d}}_s^{n+1} + \alpha_{\mathrm{m}} \ddot{\boldsymbol{d}}_s^{n} \right\rangle_{\hat{\Omega}_s} + \left\langle \hat{\nabla} \boldsymbol{\varphi}, \alpha'_{\mathrm{f}} \boldsymbol{P}(\boldsymbol{d}_s^{k+1}) + \alpha_{\mathrm{f}} \boldsymbol{P}(\boldsymbol{d}_s^{n}) \right\rangle_{\hat{\Omega}_s} \\
&= \alpha_{\mathrm{f}} \left\langle \boldsymbol{\varphi}, \boldsymbol{P}(\boldsymbol{d}_s^{n}) \hat{\boldsymbol{n}}_s \right\rangle_{\hat{\Gamma}_{R,s} \cup \hat{\Sigma}} - \alpha'_{\mathrm{f}} \left\langle \boldsymbol{\varphi}, k_e \boldsymbol{d}_s^{k+1} + c_e \dot{\boldsymbol{d}}_s^{n+1} \right\rangle_{\hat{\Gamma}_{R,s}} + \left\langle \boldsymbol{\varphi}, \alpha'_{\mathrm{f}} \boldsymbol{b}_s^{n+1} + \alpha_{\mathrm{f}} \boldsymbol{b}_s^{n} \right\rangle_{\hat{\Omega}_s} \\
&\quad + \alpha'_{\mathrm{f}} \left\langle \boldsymbol{\varphi}, \eta_s^R \left(\boldsymbol{u}_f^\star - \dot{\boldsymbol{d}}_s^{n+1} \right) + J_f \boldsymbol{\sigma}_f \left(\boldsymbol{u}_f^\star, p_f^{k+1}, \mu_f^{n+1} \right) \boldsymbol{F}_f^{-\top} \hat{\boldsymbol{n}}_s \right\rangle_{\hat{\Sigma}},
\end{aligned} \tag{44}$$

where $\ddot{\boldsymbol{d}}_s^{n+1}$ and $\dot{\boldsymbol{d}}_s^{n+1}$ are evaluated with the last iterate $\boldsymbol{d}_s^k$ in, e.g., Newton's method.

Focusing on the subproblems connected to the flow problem, we solve for the projection variable $\psi^{n+1} \in H^1(\Omega_f^t)$ given $\boldsymbol{u}_f^{n+1}$, such that $\psi^{n+1}|_{\Gamma_{N,f}^t} = 0$, and

$$\left\langle \nabla \varphi, \nabla \psi^{n+1} \right\rangle_{\Omega_f^t} = - \left\langle \varphi, \nabla \cdot \boldsymbol{u}_f^{n+1} \right\rangle_{\Omega_f^t} \qquad \forall \varphi \in H^1(\Omega_f^t),\ \varphi|_{\Gamma_{N,f}^t} = 0, \tag{45}$$

to be used as ψ^n in the next time step for divergence damping. For generalised Newtonian fluids, the dynamic viscosity $\mu_f^{n+1} \in H^1(\Omega_f^t)$ is recovered from $\boldsymbol{u}_f^\star$ using an L^2-projection of (12), i.e.,

$$\left\langle \varphi, \mu_f^{n+1} \right\rangle_{\Omega_f^t} = \left\langle \varphi, \eta \left(\dot{\gamma}(\nabla \boldsymbol{u}_f^\star) \right) \right\rangle_{\Omega_f^t} \qquad \forall \varphi \in L^2(\Omega_f^t). \tag{46}$$

To compute the pressure, we first construct continuous boundary data using the auxiliary variable ζ, projecting the Dirichlet condition (19) with given $\boldsymbol{u}_f^\star$ and μ_f^{n+1} via

$$\zeta^{n+1} = -\mu_f^{n+1} \nabla \cdot \boldsymbol{u}_f^\star + \boldsymbol{n}_f \cdot \left(2\mu_f^{n+1} \nabla^{\mathrm{S}} \boldsymbol{u}_f^\star \boldsymbol{n}_f - \boldsymbol{t}_f^{n+1} \right) \qquad \text{on } \Gamma_{N,f}^t, \tag{47}$$

and then solve for the pressure $p_f^{k+1} \in H^1(\Omega_f^t)$, such that $p_f^{k+1}|_{\Gamma_{N,f}^t} = \zeta^{n+1}$ and

$$\begin{aligned}
&\left\langle \nabla \varphi, \nabla p_f^{k+1} \right\rangle_{\Omega_f^t} = \left\langle \nabla \varphi, \boldsymbol{b}_f^{n+1} - k \tilde{c}_b^\star \boldsymbol{u}_f^\star + 2 \left(\nabla \boldsymbol{u}_f^\star \right)^\top \nabla \mu_f^{n+1} - \rho_f \nabla \boldsymbol{u}_f^\star \left(\boldsymbol{u}_f^\star - \boldsymbol{u}_m \right) \right\rangle_{\Omega_f^t} \\
&- \sum_{j=0}^{m} \left\langle \varphi \boldsymbol{n}_f, \rho_f \alpha_j^m \boldsymbol{g}_f^{n+1-j} \right\rangle_{\Gamma_{D,f}^t} - \left\langle \varphi \boldsymbol{n}_f, \rho_f \ddot{\boldsymbol{d}}_s^{n+1} \right\rangle_{\Sigma^t} + \left\langle \boldsymbol{n}_f \times \nabla \varphi, \mu_f^{n+1} \nabla \times \boldsymbol{u}_f^\star \right\rangle_{\Sigma^t \cup \Gamma_{D,f}^t}
\end{aligned} \tag{48}$$

holds for all $\varphi \in H^1(\Omega_f^t)$, where $\varphi|_{\Gamma_{N,f}^t} = 0$ and $\ddot{\boldsymbol{d}}_s^{n+1}$ is evaluated using the last computed iterate $\boldsymbol{d}_s^k$ in (39). Also, note that the reaction term stemming from the thrombus model is treated *explicitly*. Then, the fluid momentum step consists of finding $\boldsymbol{u}_f^{n+1} \in [H^1(\Omega_f^t)]^d$ with $\boldsymbol{u}_f^{n+1} = \boldsymbol{g}_f^{n+1}$ on $\Gamma_{D,f}^t$, $\boldsymbol{u}_f^{n+1} = \dot{\boldsymbol{d}}_s^{n+1}$ on Σ^t, such that

$$\begin{aligned}
&\rho_f \left\langle \boldsymbol{\varphi}, \alpha_o^m \boldsymbol{u}_f^{n+1} + \nabla \boldsymbol{u}_f^{n+1} \left(\boldsymbol{u}_f^\star - \boldsymbol{u}_m \right) \right\rangle_{\Omega_f^t} + \left\langle \nabla \boldsymbol{\varphi}, 2\mu_f^{n+1} \nabla^{\mathrm{S}} \boldsymbol{u}_f^{n+1} \right\rangle_{\Omega_f^t} + \left\langle \boldsymbol{\varphi}, k \tilde{c}_b^\star \boldsymbol{u}_f^{n+1} \right\rangle_{\Omega_f^t} \\
&= \left\langle \nabla \boldsymbol{\varphi}, p_f^{n+1} \boldsymbol{I} \right\rangle_{\Omega_f^t} - \rho_f \sum_{j=0}^{m-1} \alpha_{j+1}^m \left\langle \boldsymbol{\varphi}, \boldsymbol{u}_f^{n-j} - \nabla \psi^{n-j} \right\rangle_{\Omega_f^t} + \left\langle \boldsymbol{\varphi}, \boldsymbol{t}_f^{n+1} \right\rangle_{\Gamma_{N,f}^t} + \left\langle \boldsymbol{\varphi}, \boldsymbol{b}_f^{n+1} \right\rangle_{\hat{\Omega}_f},
\end{aligned} \tag{49}$$

holds for all $\boldsymbol{\varphi} \in [H^1(\Omega_f^t)]^d$, with $\boldsymbol{\varphi} = \mathbf{0}$ on $\Gamma_{D,f}^t \cup \Sigma^t$, where the auxiliary projection variable ψ is considered only for the past time steps' velocities and the thrombus reaction term is considered *semi-implicitly*. For details on the derivation of (43)–(49) and the corresponding reasoning behind, the interested reader is once again referred to [2, 3].

The last ingredients remaining to be specified are the weak forms corresponding to the thrombus model. The residence time depends on the fluid and mesh velocities only, which we summarise in the convective velocity $\boldsymbol{c}^{n+1} := \boldsymbol{u}_f^{n+1} - \boldsymbol{u}_m^{n+1}$ for convenience. Then, the problem is to find $\tau^{n+1} \in H^1(\Omega_f^t)$, such that $\tau|_{\Gamma_{D,f}^t} = 0$ and

$$\left\langle \varphi, \alpha_0^m \tau^{n+1} + \boldsymbol{c}^{n+1} \cdot \nabla \tau^{n+1} \right\rangle_{\Omega_f^t} + D_\tau \left\langle \nabla\varphi, \nabla\tau^{n+1} \right\rangle_{\Omega_f^t} = \langle \varphi, 1 \rangle_{\Omega_f^t} - \sum_{j=0}^{m-1} \left\langle \varphi, \alpha_{j+1}^m \tau^{n-j} \right\rangle_{\Omega_f^t} \tag{50}$$

holds for all $\varphi \in H^1(\Omega_f^t)$ with $\varphi|_{\Gamma_{D,f}^t} = 0$. The next step within the thrombus formation framework consists of solving for the activated platelets concentration, $c_a \in H^1(\Omega_f^t)$, and resting platelets concentration, $c_r \in H^1(\Omega_f^t)$, with $c_a = c_r = 0$ on $\Gamma_{D,f}^t$, such that there holds

$$\left\langle \varphi, \alpha_0^m c_a^{n+1} + \boldsymbol{c}^{n+1} \cdot \nabla c_a^{n+1} \right\rangle_{\Omega_f^t} + \left\langle \nabla\varphi, D_p^{n+1} \nabla c_a^{n+1} \right\rangle_{\Omega_f^t} = \langle \varphi, (\alpha_1 c_a^\star + \alpha_2 \overline{\tau})\, c_r^\star \rangle_{\Omega_f^t} - \sum_{j=0}^{m-1} \left\langle \varphi, \alpha_{j+1}^m c_a^{n-j} \right\rangle_{\Omega_f^t}, \tag{51}$$

$$\left\langle \varphi, \alpha_0^m c_r^{n+1} + \boldsymbol{c}^{n+1} \cdot \nabla c_r^{n+1} \right\rangle_{\Omega_f^t} + \left\langle \nabla\varphi, D_p^{n+1} \nabla c_r^{n+1} \right\rangle_{\Omega_f^t} = \langle \varphi, (\alpha_3 c_a^\star + \alpha_4 \overline{\tau})\, c_r^\star \rangle_{\Omega_f^t} - \sum_{j=0}^{m-1} \left\langle \varphi, \alpha_{j+1}^m c_r^{n-j} \right\rangle_{\Omega_f^t}, \tag{52}$$

$\forall \varphi \in H^1(\Omega_f^t)$ with $\varphi|_{\Gamma_{D,f}^t} = 0$, where D_p^{n+1} is evaluated using $\boldsymbol{u}_f^{n+1}$ and $\overline{\tau}$ refers to the past cardiac cycle's time-averaged residence time. Note here also, that these weak forms are linearised and decoupled counterparts of (29)–(32), which can be solved in any desired order.

Lastly, the concentrations of coagulant, $c_c \in H^1(\Omega)$ with $c_c|_{\Gamma_{D,f}^t} = 0$ and bound platelets, $c_b \in H^1(\Omega)$ are sought, such that $\forall \varphi \in H^1(\Omega_f^t)$ with $\varphi|_{\Gamma_{D,f}^t} = 0$, there holds

$$\left\langle \varphi, \alpha_0^m c_c^{n+1} \right\rangle_{\Omega_f^t} + \left\langle \nabla\varphi, D_c^{n+1} \nabla c_c^{n+1} \right\rangle_{\Omega_f^t} = \langle \varphi, k_c \tilde{c}_b^\star \tilde{\gamma} \rangle_{\Omega_f^t} - \sum_{j=0}^{m-1} \left\langle \varphi, \alpha_{j+1}^m c_c^{n-j} \right\rangle_{\Omega_f^t} + \langle \varphi, q_c \rangle_{\Gamma_c^t}, \tag{53}$$

$$c_b^{n+1} = k_b \tilde{c}_c^\star \tilde{\tau} \tilde{\gamma} c_a^{n+1} - \sum_{j=0}^{m-1} \alpha_{j+1}^m c_b^{n-j}, \tag{54}$$

where D_c^{n+1} is evaluated using $\boldsymbol{u}_f^{n+1}$ and the scaled quantities $\tilde{\tau}$ and $\tilde{\gamma}$ refer to the past cardiac cycle's time-averaged residence time and (L^2-projected) shear rate. Note, that (53) is a reaction–diffusion equation followed by (54), a simple time step of an implicit BDF scheme, realised via vector operations only.

With this, the final scheme consists of the following steps at time step n from t^n to t^{n+1}:

1. Extrapolate solution components in time via (42).
2. Based on $\boldsymbol{d}_s^\star$, update $\boldsymbol{d}_f^{n+1}$ via (43), the fluid domain Ω_f^t and the mesh velocity $\boldsymbol{u}_m^{n+1}$.
3. Project μ_f^{n+1} by solving (46).
4. Construct continuous boundary data ζ^{n+1} on $\Gamma_{N,f}^t$ (47).

5. *Until converged:* iterate through the PPE (3), considering the extrapolated bound platelets concentration $c_b^\star$ in $\tilde{c}_b$ in an *explicit* thrombus reaction term, and the solid momentum (44) steps, accelerating the coupling by an IQN-ILS algorithm (see [3, 8]).
6. Solve the fluid's momentum balance equation for $\boldsymbol{u}_f^{n+1}$, using the extrapolated bound platelets concentration $c_b^\star$ in $\tilde{c}_b$ and a *semi-implicit* thrombus reaction term.
7. Compute the auxiliary variable ψ^{n+1} via (45) to act on $\boldsymbol{u}_f^n$ in the next time step.
8. Update the residence time τ^{n+1} given the flow field by solving (50).
9. Determine concentrations of activated and resting platelets, c_a^{n+1} and c_r^{n+1}, via (51)–(52).
10. Solve for the coagulant concentration c_c^{n+1} using (53).
11. Perform a simple BDF time step (54) for the bound platelets concentration, based on an L^2-projected, scaled and time-averaged shear rate.

Let us note here, that all (potentially) convection-dominated problems in the semi-implicit FSI scheme involving thrombus formation, i.e., the fluid's momentum balance equation (49), the equations governing the residence time (50) and activated and resting platelets concentrations (51)–(52) are stabilised via residual-based methods [9]. To treat cases of recirculatory flow, where $\boldsymbol{u}_f \cdot \boldsymbol{n} < 0$ introduces spurious energy over $\Gamma_{N,f}^t$, backflow stabilisation [10] is added and the residence time and concentrations are weakly enforced to zero using a penalty approach.

4 NUMERICAL EXAMPLE

The implementation of the presented framework is based on `deal.II` [11], parallelised through MPI and makes heavy use of the algebraic multigrid methods provided by Trilinos' ML package [12] for preconditioning iterative solvers of all involved linear systems. Moreover, these first results presented herein are limited to two spatial dimensions because of computational complexity but nonetheless give important insights into the performance of the split-step scheme.

A channel of 10 cm length and inlet radius $R = 1$ cm with 1 mm thick elastic walls and a backward-facing flap as depicted in Fig. 1 is considered. Thrombus formation is triggered by a nonzero flux q_c in the coagulant concentration equation (53), where Γ_c^t is defined as the fluid–structure interface in the region behind the backward-facing flap.

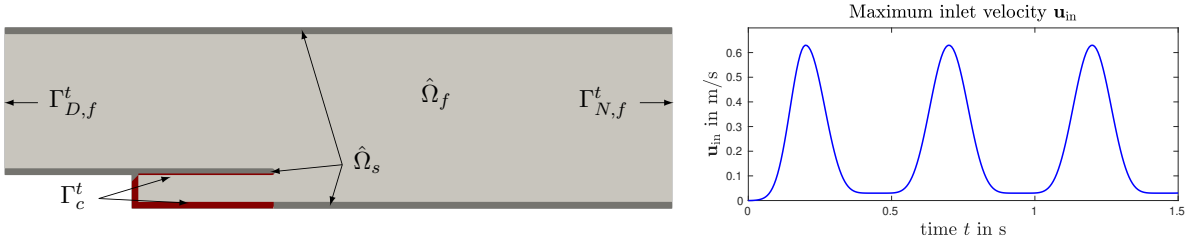

Figure 1: Channel with a backward-facing flap: initial configuration at $t = 0$ s with fluid domain $\hat{\Omega}_f$ in light grey, solid domain $\hat{\Omega}_s$ in dark grey and solid touching Γ_c^t highlighted in red (left). Ramped periodic maximum inflow velocity prescribed on the center of the channel's inlet $\Gamma_{D,f}^t$ (right).

The structure is pinned at the in- and outlet faces, making up $\hat{\Gamma}_{D,s}$ and viscoelastic support with $k_e = 2 \times 10^7$ N/m³ and $c_e = 10^5$ Ns/m³ is considered on the top and bottom of the channel.

Starting from the quiescent state, we ramp up a parabolic inflow profile centered on the left side, prescribing $\boldsymbol{u}_f = (1,0,0)^\top \boldsymbol{u}_{\text{in}}\,(1 - |y|^2/R^2)$, with the maximum inlet velocity shown in Fig. 1. On the right side of the channel, $\Gamma^t_{N,f}$, we combine nonzero traction conditions stemming from a two-element Windkessel model and backflow stabilisation,

$$\boldsymbol{t}_f^{n+1} = -p_c(Q^n)\boldsymbol{n}_f - \frac{\rho_f}{4}\boldsymbol{u}_f^{n+1}(|\boldsymbol{u}_f^\star \cdot \boldsymbol{n}_f| - \boldsymbol{u}_f^\star \cdot \boldsymbol{n}_f), \tag{55}$$

where Q^n hints at the volumetric flow rate over $\Gamma^t_{N,f}$ from the previous time step being used. The Windkessel model features a capacitance of 8×10^{-8} $\mathrm{m^4 s^2/kg}$, a distal resistance of 15×10^5 $\mathrm{kg/m^4 s}$ and a distal pressure of 7.5 kPa. For further details regarding this choice see [2].

The Carreau fluid has a density $\rho_f = 1060$ $\mathrm{kg/m^3}$ and we set upper and lower viscosity limits of $\eta_0 = 39.13$ mPa s and $\eta_\infty = 5.13$ mPa s, $\lambda_f = 0.9$ s and $\xi = 0.32$. The linear elastic solid has a density of $\rho_s = 1200$ $\mathrm{kg/m^3}$ and the Lamé parameters correspond to a Young's modulus of 100 kPa and a Poisson's ratio of 0.3. The elastic properties selected here are not resembling arterial tissue, but suffice for this initial study.

For time integration, we employ BDF-2 for the fluid and the second-order accurate CH-α scheme with $\rho_\infty = 0$ for the structural equations, while the equations governing thrombus growth are integrated via BDF-1. The time step size Δt^n is adaptively chosen, targeting an element CFL number of 0.5. Overall, 20 cardiac cycles are considered, i.e., $T = 10$ s and thrombus formation is activated from $t = T_p = 0.5$ s, where the coupling to the FSI problem is smoothly ramped from $t = T_p = 0.5$ s to fully active at $t = 2\,T_p = 1$ s.

With these settings, the semi-implicit scheme takes $\approx 34 \times 10^3$ time steps, and the fluid's pressure and the structure's displacement are solved $\approx 10^5$ times. Thus, the average iteration count is ≈ 2.95 when reducing the pressure and displacement interface norms by a factor of 10^4. Despite the high added-mass effect, adaptive time step selection, and the Windkessel model being used, the split-step scheme is robust, owing to the combination of IQN-ILS acceleration and Robin interface conditions with $\eta_s^R := \rho_f/\Delta t^n$.

In Fig. 2, the displacement norm $||\boldsymbol{d}_f||$ and pressure p_f in point A at the tip of the beam are shown. Rather large displacements are seen, caused by (i) the pressure fluctuations at the outlet and (ii) the structure's compressibility. The FSI iteration counts are rather uniform, showing only a slight decrease towards the end of the considered time interval when the thrombus slowly reaches its maximum extent.

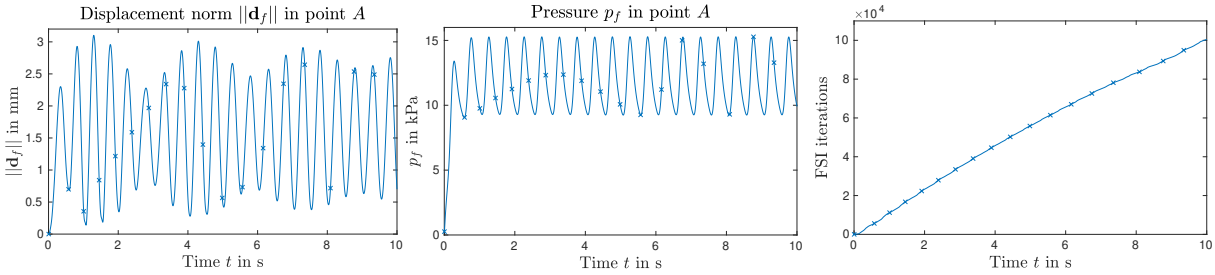

Figure 2: Channel with a backward-facing flap: displacement (left) and pressure (middle) in point A at the tip of the beam and FSI iterations (right) over time.

As expected, the thrombus – the concentration of bound platelets c_b – builds up in the region

below the flap, where low shear rates are present and Γ_c^t is defined. As shown in Fig. 3, the region occupied by thrombus extends also towards the end of the channel in the wake of the backward-facing flap until it stagnates due to high shear. Initially, slight oscillations in c_b are seen, caused by a rather coarse spatial resolution employed beneath the flap.

The pressure fluctuations cause a compression of the flap and expansion of the channel, while the stagnating fluid (low μ_f due to low $\dot{\gamma}$) below the flap suppresses excessive flap motion due to incompressibility. Moreover, we see a strong impact on the flow field as the concentration of bound platelets increases – the thrombus reaction term hinders fluid flow, such that in the wake of the flap where the thrombus builds up, the fluid flow is restricted. Comparing cycles 2 and 17 in Fig. 4, a striking difference in the flow fields is observed.

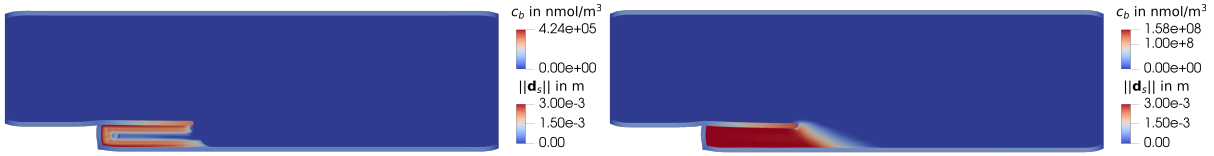

Figure 3: Concentration of bound platelets c_b in Ω_f^t and displacement norm in Ω_s^t at late diastole in cycles 2 ($t \approx 0.87$ s, left) and 17 ($t \approx 9.30$ s, right).

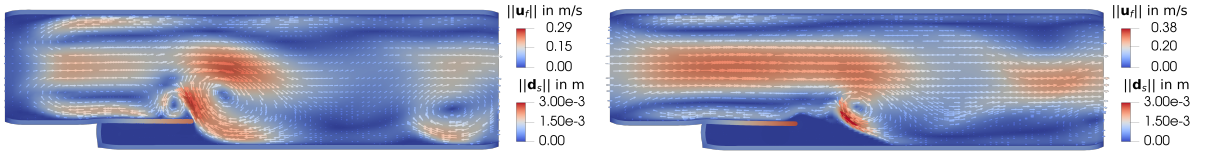

Figure 4: Fluid velocity $\boldsymbol{u}_f$ in Ω_f^t and displacement norm in Ω_s^t at late diastole in cycles 2 ($t \approx 0.87$ s, left) and 17 ($t \approx 9.30$ s, right).

5 CONCLUDING REMARKS

We present a semi-implicit FSI scheme incorporating the thrombus formation model by Menichini et al. [1], allowing for the coupled simulation of structural displacements, incompressible flow of generalised Newtonian fluids, and thrombus constituents in an added-mass stable fashion. Based on a pressure Poisson equation, the scheme couples merely the fluid pressure and structural displacements iteratively, while the remaining equations are only solved once per time step. First promising results in a two-dimensional setting are carried out, showing the applicability of the method to clinically relevant settings being the focus of ongoing work.

REFERENCES

[1] C. Menichini, X.Y. Xu, Mathematical modeling of thrombus formation in idealized models of aortic dissection: initial findings and potential applications. *J. Math. Biol.*, Vol. **73**(5), pp. 12051226, 2016.

[2] R. Schussnig, D.R.Q. Pacheco, T.-P. Fries, Efficient split-step schemes for fluid–structure interaction involving incompressible generalised Newtonian flows, *Comput. Struct.*, Vol. **260**, pp. 106718, 2022.

[3] R. Schussnig, D.R.Q. Pacheco, M. Kaltenbacher, T.-P. Fries, Semi-Implicit Fluid–Structure Interaction in Biomedical Applications, *Comput. Methods Appl. Mech. Eng.*, submitted.

[4] D.R.Q. Pacheco, R. Schussnig and T.-P. Fries, An efficient split-step framework for non-Newtonian incompressible flow problems with consistent pressure boundary conditions, *Comput. Methods Appl. Mech. Eng.*, Vol. **382**, pp. 113888, 2021.

[5] T. Wick, Fluid-structure interactions using different mesh motion techniques, *Comput. Struct.*, Vol. **89**, pp. 1456–1467, 2011.

[6] S. Badia, F. Nobile, C. Vergara, Fluid–structure partitioned procedures based on Robin transmission conditions, *J. Comput. Phys.*, Vol. **227**(14), pp. 7027–7051, 2008.

[7] J. Chung, G.M. Hulbert, A time integration algorithm for structural dynamics with improved numerical dissipation: The generalized-α method, *J. Appl. Mech. Trans. ASME*, Vol. **60**(2), pp. 371–375, 1993.

[8] J. Degroote, K.-J. Bathe, J. Vierendeels, Performance of a new partitioned procedure versus a monolithic procedure in fluid–structure interaction, *Comput. Struct.*, Vol. **87**(11-12), pp. 793–801, 2009.

[9] T.J.R. Hughes, L.P. Franca, A new finite element formulation for computational fluid dynamics: VII. The Stokes problem with various well-posed boundary conditions: Symmetric formulations that converge for all velocity/pressure spaces, *Comput. Methods Appl. Mech. Eng.*, Vol. **65**(1), pp. 85–96, 1987.

[10] Ch.-H. Bruneau, P. Fabrie, Effective downstream boundary conditions for incompressible Navier–Stokes equations, *Int. J. Numer. Meth. Fluids*, Vol. **19**(8), pp. 693–705, 1994.

[11] D. Arndt, W. Bangerth, B. Blais, M. Fehling, R. Gassmöller, T. Heister, L. Heltai, U. Köcher, M. Kronbichler, M. Maier, P. Munch, J.-P. Pelteret, J.-P., S. Proell, K. Simon, B. Turcksin, D. Wells, J. Zhang, The `deal.II` library, Version 9.3, *J. Numer. Math.*, Vol. **29**(3), pp. 171–186, 2021.

[12] M.A. Heroux, J.M. Willembring, A new overview of the Trilinos project, *Sci. Program.*, Vol. **20**(2), pp. 83–88, 2012.